Thermo-Wetting and Friction Reduction Characterization of Microtextured Superhydrophobic Surfaces

Tae Jin Kim

Ravitej Kanapuram

Arnav Chhabra

Carlos Hidrovo[1]
e-mail: hidrovo@mail.utexas.edu

Department of Mechanical Engineering,
The University of Texas at Austin,
1 University Station C2200,
Austin, TX 78712

Microtextured superhydrophobic surfaces have shown potential in friction reduction applications and could be poised to make a significant impact in thermal management applications. The purpose of this paper is to account for the thermal effects of the heated fluid flowing in superhydrophobic microfluidic channels. Through microscopic observation and flow rate measurements it was observed that (1) heating may prolong the Cassie state even under elevated pressure drops by increasing the temperature in the gas layer and that (2) excessive heating may pinch the microchannel flow due to the air layer invading into the liquid layer.
[DOI: 10.1115/1.4007604]

Keywords: superhydrophobic surfaces, microchannel, thermal effects, pinching, friction

1 Introduction

Superhydrophobic surfaces that induce slip have recently received attention as a means of achieving surface friction and drag reduction [1–4]. Other applications of using such surfaces include frost prevention on aircraft flight surfaces to self-cleaning features on solar energy panels [1,5].

One way to achieve superhydrophobicity is through the microgeometry modification of low energy surfaces. Two models represent the wetting behavior of such microtextured surfaces: the Wenzel state [6] and the Cassie–Baxter state [7]. The Wenzel state models the amplifying effect that surface texturing has on the Young's contact angle under fully liquid imbibed conditions. The Cassie–Baxter state models the macroscopic contact angle formed when air pockets exist within the microtexturing. The presence of these air pockets in the Cassie state can lead to friction and drag reduction [8–10], with research in this area being actively pursued. Such research includes modeling the fluid flow over textured surfaces [11], studying the drag reduction of flow over nanotextured surfaces [12,13], and the use of chemical coatings in microtextured surfaces to enhance superhydrophobic effects [4,14]. Studies have also been conducted in utilizing thermally sensitive chemical polymers in order to modify the substrate surface energy [15].

Despite the vast literature on friction and drag reduction from superhydrophobic surfaces, there is very little work aimed at correlating the pressure and thermal effects on the stability and characteristics of this condition. While studies have shown the dependence of the overall convective heat transfer rate on slip length [16–18], experimental studies on the reverse influence that thermal effects have on the trapped gas layer and corresponding friction in superhydrophobic microchannels have not been conducted.

In this paper, microgaps are used as the surface texturing in the microchannel, and the air pockets are observed under heated conditions to study the thermal effects on the stability of the Cassie state and its friction reduction characteristics. While the water flowing in the microchannels penetrated into the microcavity gaps as the inlet pressure was increased, the penetrating water layer was pushed back to its original state as the microfluidic channel was heated due to the expanding air pockets trapped in the microgaps. Consequently, the air gaps withstood higher liquid pressure, thus, prolonging the two phase flow in the microfluidic channel. Although the experimental data indicate that heated cavities provide more stability to the Cassie state under pressure flow conditions, careful control of the microchannel heating is required since elevated temperatures resulted in a pinched liquid flow due to excessive growth of the air layer into the water layer.

2 Theoretical Model

In order to ensure a proper two phase flow through friction reduction in the microchannel flow, a microtextured surface that induces a stable Cassie state is desirable. The liquid meniscus resting on top of a textured surface is under a Cassie state if the liquid does not wet the gaps beneath the liquid interface. As a result the liquid resting on top of the textured surface will experience a reduced surface resistance since a portion of the contact surface underneath is filled with gas. The conventionally used Cassie–Baxter model [4] is

$$\cos\theta_{CB} = \phi_s \cos\theta_Y - (1 - \phi_s) \tag{1}$$

where θ_{CB} is the Cassie–Baxter angle, θ_Y is the Young's contact angle, and ϕ_s is the ratio of solid contact area to the nominal area. Also, in order to maintain the air–water interface, the surface topography must be in the stable Cassie state [19], or rougher than the critical roughness factor [20]

$$r_c = \phi_s - \frac{1 - \phi_s}{\cos\theta_Y} \tag{2}$$

where r_c is the critical roughness factor. A roughness factor lower than r_c will result in a Wenzel state where full wetting of the microtextured surface will occur, or a metastable Cassie state where the liquid initially under Cassie state may transition to Wenzel state if disturbances occur. On the other hand, a roughness factor higher than r_c will lead to a stable Cassie state. In our experiments, we have conducted tests on textured microfluidic channels with roughness factors significantly higher than the critical roughness factor.

3 Experimental Setup

3.1 Fabrication of the Microcavity Substrate Microchannels. The microfluidic devices were fabricated by soft-lithography (Fig. 1). A bare wafer was coated with SU-8 2050 (Microchem) and a negative mold for the polydimethylsiloxane (PDMS) microfluidic channel was fabricated through standard photolithographic procedures. The thickness of the SU-8 mold pattern was measured using a profilometer (Veeco) to confirm the channel thickness. The wafer was then silanized (UCT Specialties, LLC) for at least an hour in a vacuum desiccator to fluorinate the SU-8 mold. A PDMS base and solvent (Dow Corning) mixture, at a volume ratio of 10:1, was poured on the silanized SU-8 mold. The entire wafer was cured at 95 °C for 2 h. The cured PDMS microfluidic channel

[1]Corresponding author.

Contributed by the Fluids Engineering Division of ASME for publication in the JOURNAL OF FLUIDS ENGINEERING. Manuscript received March 23, 2012; final manuscript received September 3, 2012; published online October 23, 2012. Assoc. Editor: Peter Vorobieff.

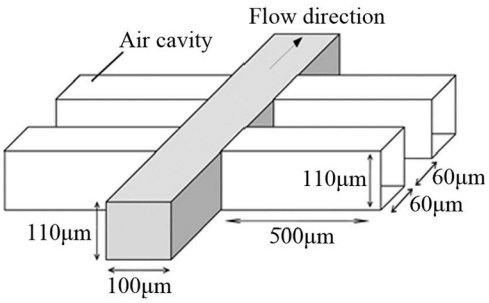

Fig. 1 Schematic diagram of 60 μm × 500 μm trenched microfluidic channel

replicas were peeled off from the wafer and were bonded to glass substrates. Prior to bonding, the glass substrates were spin coated with a thin layer of PDMS to ensure uniform properties within the microfluidic channel. Both PDMS slabs and PDMS coated glass substrates were treated with oxygen plasma (Harrick Plasma) at 29Watts for 20 s. Once the bonding was complete, the treated samples were then baked overnight on a hot plate at 65 °C.

The channel dimension for the baseline channel with no surface textures is 100 μm × 110 μm × 2 cm (width × height × length). For the channels with microtextured surface, the liquid flow channel dimension is similar to the baseline channel and an array of microtrenches with dimensions of 60 μm × 500 μm (gap size × depth of cavity) on the side walls are added.

3.2 Heating of the Microfluidic Channel. A water reservoir with a controllable column height was used to generate a constant pressure source (Fig. 2). The water column device was connected to the inlet of the microchannels, and constant pressure conditions of 2500 Pa, 3500 Pa, and 4500 Pa were applied to the microfluidic channel by controlling the water column height. A pressure transducer (Omega) was used to measure the gauge water pressure supplied to the channel.

A resistive heating pad was placed directly underneath the microfluidic device to provide a constant heat flux to the channel. The heat transfer rate was controlled by varying the voltage to the heat pad. Under a fixed pressure head, the liquid–gas interface

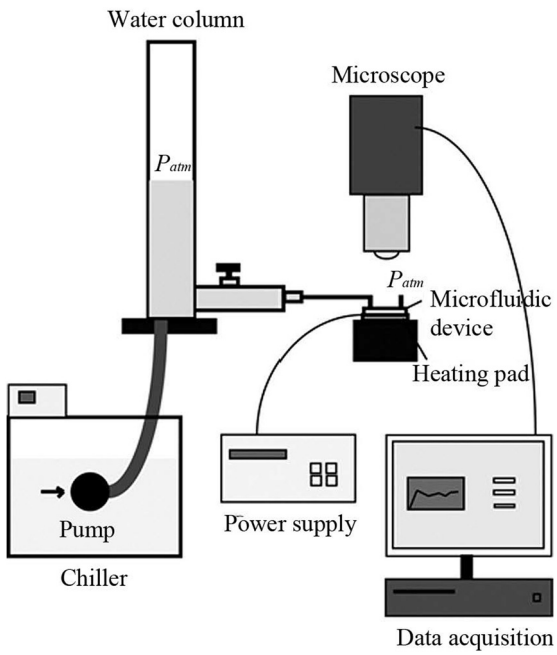

Fig. 2 Experimental setup of pressure measurement test

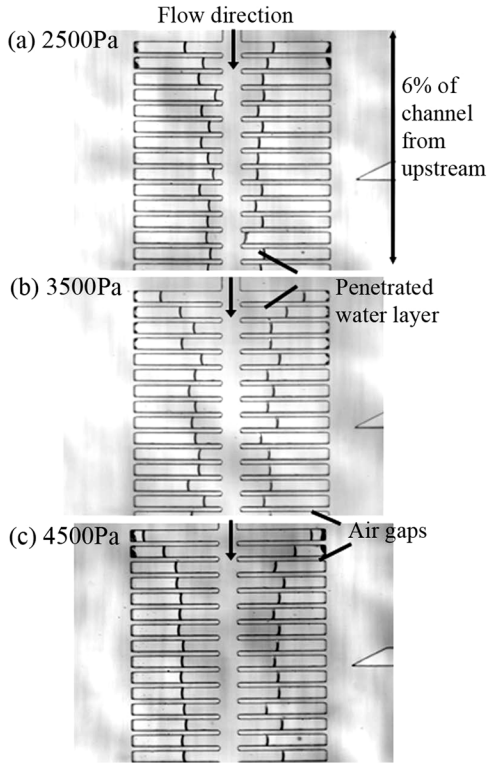

Fig. 3 Micrographs of 60 μm × 500 μm trenched channel under (*a*) 2500 Pa, (*b*) 3500 Pa, and (*c*) 4500 Pa (5×) at 25 °C. Penetration of the water layer into the microcavities can be observed near the inlet.

was initially observed under unheated conditions. Then, the temperature of the bottom substrate was increased from 26 °C to 32 °C, with increments of 1 °C. Measurements were performed with a microscope after the substrate temperature was stabilized.

4 Results

4.1 Heating Effects on Penetration Depth. Water flow in the microfluidic channel was generated by a constant pressure source. With a constant pressure applied to the microfluidic channel, the pressure is ρgh at the inlet and is assumed to drop linearly to the outlet pressure. Depending on the inlet pressure, this pressure gradient will either wet the cavity or maintain the Cassie state. Since the pressure required to prevent penetration throughout the entire channel is calculated to be 1000 Pa, the inlet pressures were large enough (2500 Pa, 3500 Pa, and 4500 Pa) to induce penetration near the inlet region, as can be seen in Fig. 3. The images in Fig. 3 visually depict the relationship between pressure and penetration depth in the cavities, where the penetration depth is measured using a microruler. The pressure is the largest near the inlet and the smallest near the outlet.

However, as heat was applied to the channel, the gas layer started to expand with increasing temperature. For the case where the substrate temperature was 28 °C, the curvature of the penetrating liquid interface was convex, indicating that the liquid pressure is greater than the gas pressure. As the substrate temperature reached 30 °C (Fig. 4), the curvature gradually reduced to a near flat shaped profile, and at 32 °C the curvature was reversed to a concave profile. Once the curvature was reversed, it was apparent that the penetrated liquid started to retract because of the expanding air pockets. This indicates that the temperature of the gas layer was high enough that the pressure of the gas pocket became greater than that of the water layer.

The penetration depth as a function of channel location under different temperature conditions is presented in Fig. 5, where the

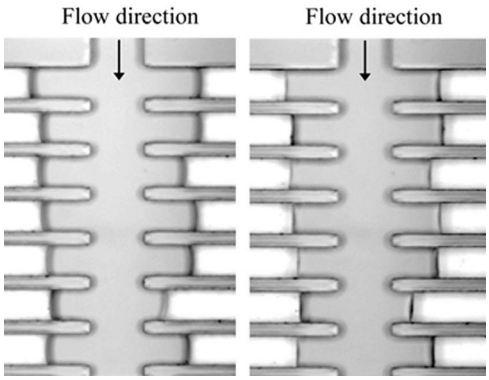

Fig. 4 Micrographs (near the inlet) of heating effects on liquid penetration at (*a*) 30 °C and (*b*) 32 °C. The inlet pressure is at 2400 Pa (gauge).

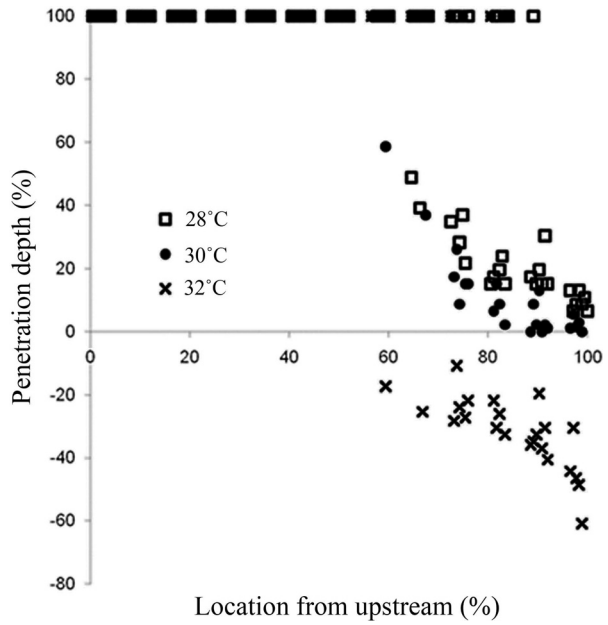

Fig. 5 Penetration depth versus location under different substrate temperature conditions. The inlet pressure is at 3200 Pa (gauge).

inlet pressure was fixed at 3200 Pa. From the graph, it is apparent that the penetration depth along the channel decreased as the temperature was increased.

At 28 °C, 100% of the cavities were penetrated, where approximately 60% of the cavities were fully wetted. As the temperature was increased to 30 °C, the penetration depth started to decrease as the gas layer expanded due to the increase in gas pressure. Approximately 10% of the channel showed that the liquid layer retracted back to a nonpenetrating state. It should be noted that the fully wetted cavities throughout 60% of the channel remain fully wetted. When the temperature was increased to 32 °C, the gas layer expanded further and the partially wetted cavities transitioned to a fully nonwetted state. For this case, the gas layer continued to expand and started to invade the liquid layer instead.

From the above results, it can be seen that the liquid penetration can be prevented by heating the air trapped within the microcavities. With sufficient heating, penetration can be prevented even under higher liquid pressures. However, with the current pressure range, the effect of prolonging the Cassie state did not significantly affect the friction in the channel. By testing at higher pressure range, it may be possible to achieve reduced frictional effect in the heated channel.

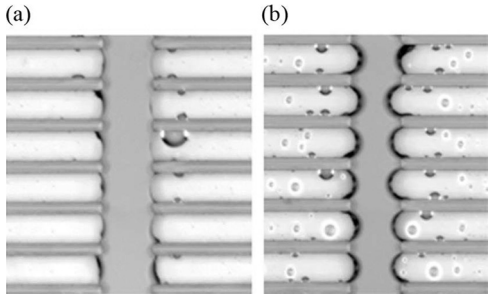

Fig. 6 Micrographs (near the outlet) of heating effects on liquid penetration at (*a*) 30 °C and (b) 32 °C. The inlet pressure is at 2400 Pa (gauge).

4.2 Pinching Effects and Flow Rate Reduction. At increased temperatures, the growth of the air layer continued until it invaded the main channel, where the air pocket growth is presented in Fig. 5 as the negative penetration depth, and the liquid flow started to experience a "pinching" effect due to the reduced cross-sectional area of the flow (Fig. 6). This pinching effect is analogous to a closing valve. At lower inlet pressures, even a slight increase in temperature resulted in a reduced flow rate until the flow was eventually disrupted (Fig. 7). For higher inlet pressures, the flow rate was maintained at higher temperatures. However, once the temperature reached a certain threshold, the pressure in

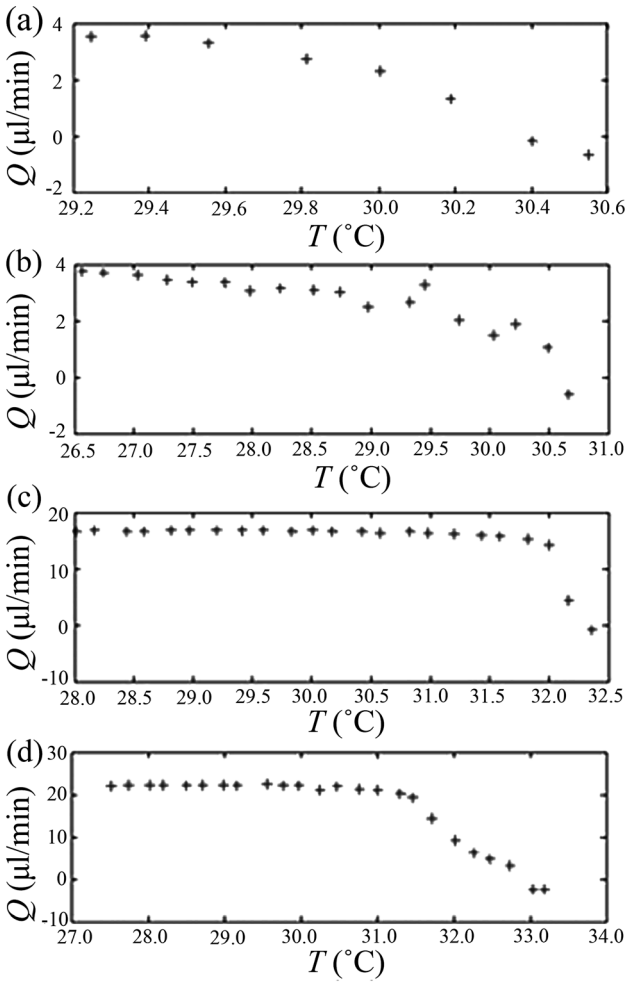

Fig. 7 Flow rate versus temperature graph of 60 μm × 500 μm cavity channels under (*a*) 800 Pa, (*b*) 1600 Pa, (*c*) 2400 Pa, and (*d*) 3200 Pa inlet pressures

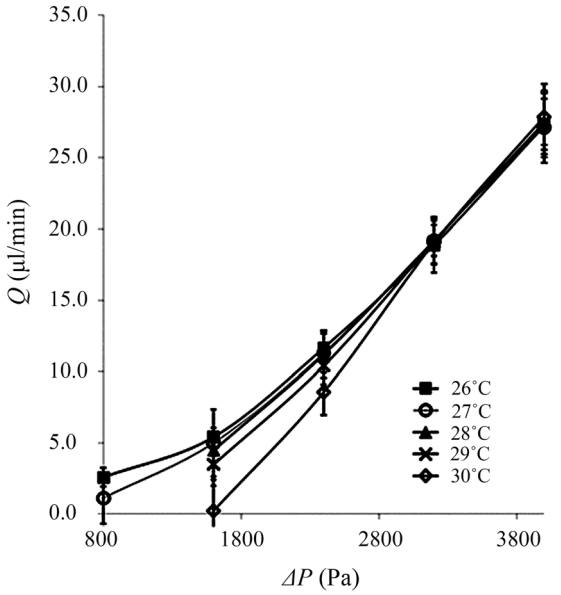

Fig. 8 Flow rate versus ΔP graph of 60 μm × 500 μm cavity channels under different heat substrate temperatures

the air pockets exceeded the liquid pressure and a drastic drop in flow rate was observed. This phenomenon can also be observed in Fig. 8. At lower pressures, the flow rate was very sensitive to the change in temperature. For this case, the air pockets expanded even under a slight increase in temperature. It was observed that the liquid flow was disrupted at a substrate temperature of 28 °C.

Current analytical/numerical models [21–23] estimate the effective slip length based on the assumption that the air–water interface is a shear-free boundary condition. This is an idealized assumption that can lead to estimated slip lengths quite different from those observed experimentally [2,10,24–26]. Furthermore, recent results suggest that for isolated gas pocket microgeometries the air–water interface behaves closer to a no-slip boundary condition than a shear-free one [27]. As such even a slight growth of air layer into the water layer leads to a substantial and detrimental flow reduction and, consequently, higher friction. The pinching effects presented here seem to validate this notion that the air–water interface cannot simply be modeled as a shear-free boundary.

While it has been suggested that the local flow behavior near the microtextured walls may affect the convective heat transfer rate [28], the results presented here also suggest that heat transfer may in turn affect the slip length, particularly for microchannel flow over microtextured walls with isolated air pockets. As such, temperature should be carefully monitored and controlled in these systems as heating might either prolong the stability of the Cassie state or aversely pinch the flow and increase friction if excessively heated, which can in turn lead to a decrease of the convective heat transfer rate.

5 Conclusion

In this paper we investigated the heating effects of the air pockets trapped between the roughness elements in a microchannel flow. The side walls of the PDMS microchannels were grooved to form air pockets in the liquid channel flow.

A constant pressure source was used to flow water into the microfluidic channel and the flow rate was measured using a flow meter. It was observed that the flow rate for microchannels with microcavities on the side walls increased under heated conditions, where the air–liquid interface in the heated channels withstood higher pressure ranges than the unheated channels. It was also observed that the penetrated liquid layer was pushed back due to the expanding gas layer if the heat transfer was increased. This is the result of a penetration resistance effect arising from the compressibility of the entrapped air as a function of temperature.

The results indicate that the Cassie state can be prolonged if the air cavities are heated and that surfaces with isolated air pockets may actually be more stable than surfaces with nonisolated air pockets. Hence, we anticipate that the thermal effect of air pockets can be extended to the designing of superhydrophobic surfaces exposed to highly pressurized conditions. Nonetheless, careful control of the microchannel heating is required since excessive heating incurs pinching of the flow, thus significantly increasing the microchannel friction. Further experiments on flow visualization under heated conditions are required to quantify the slip lengths and its relation to the convective heat transfer.

Acknowledgment

This work was funded by The University of Texas at Austin start-up funds and The University of Texas System Science and Technology Acquisition and Retention funds.

Nomenclature

Q = flow rate
r_c = critical roughness
T = temperature
ΔP = differential pressure
ϕ_s = solid contact area ratio
θ_{CB} = Cassie–Baxter angle
θ_Y = Young's contact angle

References

[1] Ma, M., and Hill, R. M., 2006, "Superhydrophobic Surfaces," Curr. Op. Colloid In., **11**(4), pp. 193–202.
[2] Choi, C. H., Ulmanella, U., Kim, J., Ho, C. M., and Kim, C. J., 2006, "Effective Slip and Friction Reduction in Nanograted Superhydrophobic Microchannels," Phys. Fluid., **18**(8), p. 087105.
[3] Udagawa, H., 1999, "Drag Reduction of Newtonian Fluid in a Circular Pipe With a Highly Water-Repellent Wall," J. Fluid Mech, **381**, pp. 225–238.
[4] Ou, J., Perot, B., and Rothstein, J. P., 2004, "Laminar Drag Reduction in Microchannels Using Ultrahydrophobic Surfaces," Phys. Fluid., **16**(12), pp. 4635–4643.
[5] Furstner, R., Barthlott, W., Neinhuis, C., and Walzel, P., 2005, "Wetting and Self-Cleaning Properties of Artificial Superhydrophobic Surfaces," Langmuir, **21**(3), pp. 956–961.
[6] Wenzel, R. N., 1936, "Resistance of Solid Surfaces to Wetting by Water," Ind. Eng. Chem., **28**(8), pp. 988–994.
[7] Cassie, A. B. D., and Baxter, S., 1944, "Wettability of Porous Surfaces," Trans. Faraday Soc., **40**, pp. 546–551.
[8] Carlborg, C. F., Stemme, G., and van der Wijngaart, W., 2009, "Microchannels With Substantial Friction Reduction at Large Pressure and Large Flow," IEEE 22nd International Conference on Micro Electro Mechanical Systems (MEMS 2009), Sorrento, Italy, pp. 39–42.
[9] Rothstein, J. P., 2010, "Slip on Superhydrophobic Surfaces," Annu. Rev. Fluid Mech., **42**, pp. 89–109.
[10] Truesdell, R., Mammoli, A., Vorobieff, P., van Swol, F., and Brinker, C. J., 2006, "Drag Reduction on a Patterned Superhydrophobic Surface," Phys. Rev. Lett., **97**(4), p. 044504.
[11] Cottin-Bizonne, C., Barentin, C., Charlaix, E., Bocquet, L., and Barrat, J. L., 2004, "Dynamics of Simple Liquids at Heterogeneous Surfaces: Molecular-Dynamics Simulations and Hydrodynamic Description," Eur. Phys. J. E, **15**(4), pp. 427–438.
[12] Joseph, P., Cottin-Bizonne, C., Benoit, J. M., Ybert, C., Journet, C., Tabeling, P., and Bocquet, L., 2006, "Slippage of Water Past Superhydrophobic Carbon Nanotube Forests in Microchannels," Phys. Rev. Lett., **97**(15), p. 156104.
[13] Lee, C., and Kim, C. J., 2009, "Maximizing the Giant Liquid Slip on Superhydrophobic Microstructures by Nanostructuring Their Sidewalls," Langmuir, **25**(21), pp. 12812–12818.
[14] Bahadur, V., and Garimella, S. V., 2008, "Electrowetting-Based Control of Droplet Transition and Morphology on Artificially Microstructured Surfaces," Langmuir, **24**(15), pp. 8338–8345.
[15] Sun, T., Wang, G., Feng, L., Liu, B., Ma, Y., Jiang, L., and Zhu, D., 2004, "Reversible Switching Between Superhydrophilicity and Superhydrophobicity," Ang. Chem. Int. Ed., **43**(3), pp. 357–360.
[16] Enright, R., Hodes, M., Salamon, T. R., and Muzychka, Y., 2010, "Analysis and Simulation of Heat Transfer in a Superhydrophobic Microchannel," 14th ASME International Heat Transfer Conference, Washington, DC, Vol. 6, pp. 157–168.

[17] Maynes, D., Webb, B., and Soloviev, V., 2011, "Analysis of Laminar Slip-Flow Thermal Transport in Microchannels With Transverse Rib and Cavity Structured Superhydrophobic Walls at Constant Heat Flux," 8th ASME/JSME Thermal Engineering Joint Conference, Honolulu, HI, p. T10120
[18] Maynes, D., Webb, B., and Davies, J., 2008, "Thermal Transport in a Microchannel Exhibiting Ultrahydrophobic Microribs Maintained at Constant Temperature," ASME J. Heat Transfer, **130**(2), p. 022402.
[19] Lafuma, A., and Qu, D., 2003, "Superhydrophobic States," Nat. Mater., **2**(7), pp. 457–460.
[20] Kim, T. J., and Hidrovo, C. H., 2010, "Stability Analysis of Cassie–Baxter State Under Pressure Driven Flow," 8th ASME International Conference on Nanochannels, Microchannels, and Minichannels, Montreal, QC, Canada, pp. 1657–1662.
[21] Philip, J. R., 1972, "Flows Satisfying Mixed No-Slip and No-Shear Conditions," Zeitschrift für Angewandte Mathematik und Physik, **23**(3), pp. 353–372.
[22] Cottin-Bizonne, C., Barentin, C., and Bocquet, L., 2012, "Scaling Laws for Slippage on Superhydrophobic Fractal Surfaces," Phys. Fluid., **24**(1), p. 012001.
[23] Lauga, E., and Stone, H. A., 2003, "Effective Slip in Pressure-Driven Stokes Flow," J. Fluid Mech., **489**(1), pp. 55–77.
[24] Byun, D., Kim, J., Ko, H. S., and Park, H. C., 2008, "Direct Measurement of Slip Flows in Superhydrophobic Microchannels With Transverse Grooves," Phys. Fluid., **20**(11), p. 113601.
[25] Gogte, S., Vorobieff, P., Truesdell, R., Mammoli, A., van Swol, F., Shah, P., and Brinker, C. J., 2005, "Effective Slip on Textured Superhydrophobic Surfaces," Phys. Fluid., **17**(5), p. 051701.
[26] Ou, J., and Rothstein, J. P., 2005, "Direct Velocity Measurements of the Flow Past Drag-Reducing Ultrahydrophobic Surfaces," Phys. Fluid, **17**(10), p. 103606.
[27] Kim, T. J., and Hidrovo, C. H., "Pressure and Partial Wetting Effects on Superhydrophobic Friction Reduction in Microchannel Flow," Phys. Fluid (accepted).
[28] Williams, A., Vorobieff, P., and Mammoli, A., 2012, "Effect of Slip Flow on Heat Transfer: Numerical Analysis," 50th AIAA Aerospace Sciences Meeting including the New Horizons Forum and Aerospace Exposition, Nashville, TN, pp. 1–11.